



HAL
open science

Cesium Rydberg states ionization study by 3-D ion-electron correlation

R Hahn, A. Trimeche, C. Lopez, D. Comparat, Y. J. Picard

► **To cite this version:**

R Hahn, A. Trimeche, C. Lopez, D. Comparat, Y. J. Picard. Cesium Rydberg states ionization study by 3-D ion-electron correlation. 2020. hal-03017763

HAL Id: hal-03017763

<https://hal.science/hal-03017763>

Preprint submitted on 23 Nov 2020

HAL is a multi-disciplinary open access archive for the deposit and dissemination of scientific research documents, whether they are published or not. The documents may come from teaching and research institutions in France or abroad, or from public or private research centers.

L'archive ouverte pluridisciplinaire **HAL**, est destinée au dépôt et à la diffusion de documents scientifiques de niveau recherche, publiés ou non, émanant des établissements d'enseignement et de recherche français ou étrangers, des laboratoires publics ou privés.

Cesium Rydberg states ionization study by 3-D ion-electron correlation

R. Hahn[†], A. Trimeche[†], C. Lopez, D. Comparat, and Y. J. Picard^{*}
Université Paris-Saclay, CNRS, Laboratoire Aimé Cotton, 91405, Orsay, France.

[†] *These authors contributed equally to this work*

(Dated: November 23, 2020)

We study the excitation and ionization of cesium Rydberg states in an electric field (~ 2200 V/cm) near the classical field ionization threshold (~ -280 cm⁻¹ binding energy at this field) by 3-D ion-electron coincidence spectroscopy. Cesium atoms are produced by an effusive oven and excited with lasers to Stark-shifted Rydberg states or directly ionised. Using a double Time of Flight setup we record 3-D (X, Y, Time of Flight) coincidence imaging of cesium produced electrons and ions. Above-threshold photo-ionisation creates broad images with poor electron/ion-coordinates correlation. Depending on the coupling of particular Rydberg states to the continuum, various images and correlations are observed. Fast ionising states show very good correlations and reveal the electric field lines, creating an efficient electric field mapping of the ionisation region. Slow ionising states show that the relatively high atomic velocity is detrimental to the correlations. Experimental data are accurately reproduced by detailed Monte Carlo excitation and ionization simulations based on Stark maps obtained with local-frame transformation (LFT) theory. Spectroscopic LFT agreement is usually very good with better than hundreds of MHz accuracy but on particular states several GHz discrepancy is found. The study can be used to select appropriate states for the creation of ion and electron beams with high brightness, good correlation and low energy dispersion, as well as to provide a detailed analysis of LFT-theory shortcomings.

I. INTRODUCTION

Rydberg states of alkali metal atoms present strong similarities with hydrogen atoms. However, under an electric field, the presence of a polarizable core induces couplings between hydrogenic states that deeply modify the Stark diagram, the photoabsorption spectrum as well as the field ionization lifetimes [1]. For instance, alkali metal atoms ionize typically at the so called classical ionisation field $F = 1/16n^{*4}$ (in atomic units) where n^* is the effective quantum number that is linked to the binding energy of the states in zero field $E = 1/2n^{*2}$; whereas many of the Stark states of hydrogen with energies well above the classical ionization threshold are considered stable [1–5]. The behaviour of atoms under electric fields near their threshold is well known and various different species have been studied: Rb [6, 7], Na [8, 9], He [10, 11] or Ba [12], featuring observations of unstable levels crossings and interference narrowing effects. However, almost no study on Cs exists [13–15]. This is unfortunate because Cs atoms, being the heavier (stable) alkali metal atoms, have the strongest relativistic (such as spin-orbit) couplings, resulting in exaggerated behaviour compared to other alkali metal atoms. An improved comprehension of the ionisation rates in this energy region would allow the prediction of the ionisation rate of a given Stark shifted Rydberg state which is not easy, as standard matrix diagonalisation technique does not give insights into ionisation [16]. Introducing complex absorbing potentials in the Hamiltonian has shown good results in the prediction of ionisation rate in Rubidium[17], but this demands

the introduction of field-dependent parameters. Local-frame transformation theory[18] is particularly adapted to treat this problem, and naturally gives the ionisation rate of individual states through their linewidths.

We report in this work on a detailed experimental study of the lifetime of Cs Rydberg states with $n \sim 25$, near the classical ionisation threshold (laser wavelength of ~ 794 nm) in a static electric field of $F \sim 2200$ V/cm. The experimental set-up is a recently developed coincidence spectrometer (see Fig. 1(a) and ref. [19]) based on time-position-sensitive detectors (TPSD), allowing 3-D correlation imaging of the ionisation region and the production of beams of correlated ions and electrons. It has both time-of-flight (ToF) and spatial imaging capabilities that allow precise electric field mapping, study of the ionization time for slow ionization process as well as of the photo-ionisation kick-energy. Numerous states have been studied, and only typical cases are presented in this work. Accurate simulations based on realistic electric field lines and theoretical Stark maps help us to relate the observed images with individual ionisation rate. Section II presents the experimental set-up, that is calibrated using above-threshold photo-ionisation data presented in section III. Section IV presents detailed analysis of several typical cases, from fast to slow ionising states. Critical assessment of local-frame transformation (LFT)-theory performance is also presented. We conclude in section V about the applicability of this method to choose an appropriate state for high-performance electron or ion sources.

^{*} Corresponding author: daniel.comparat@universite-paris-saclay.fr

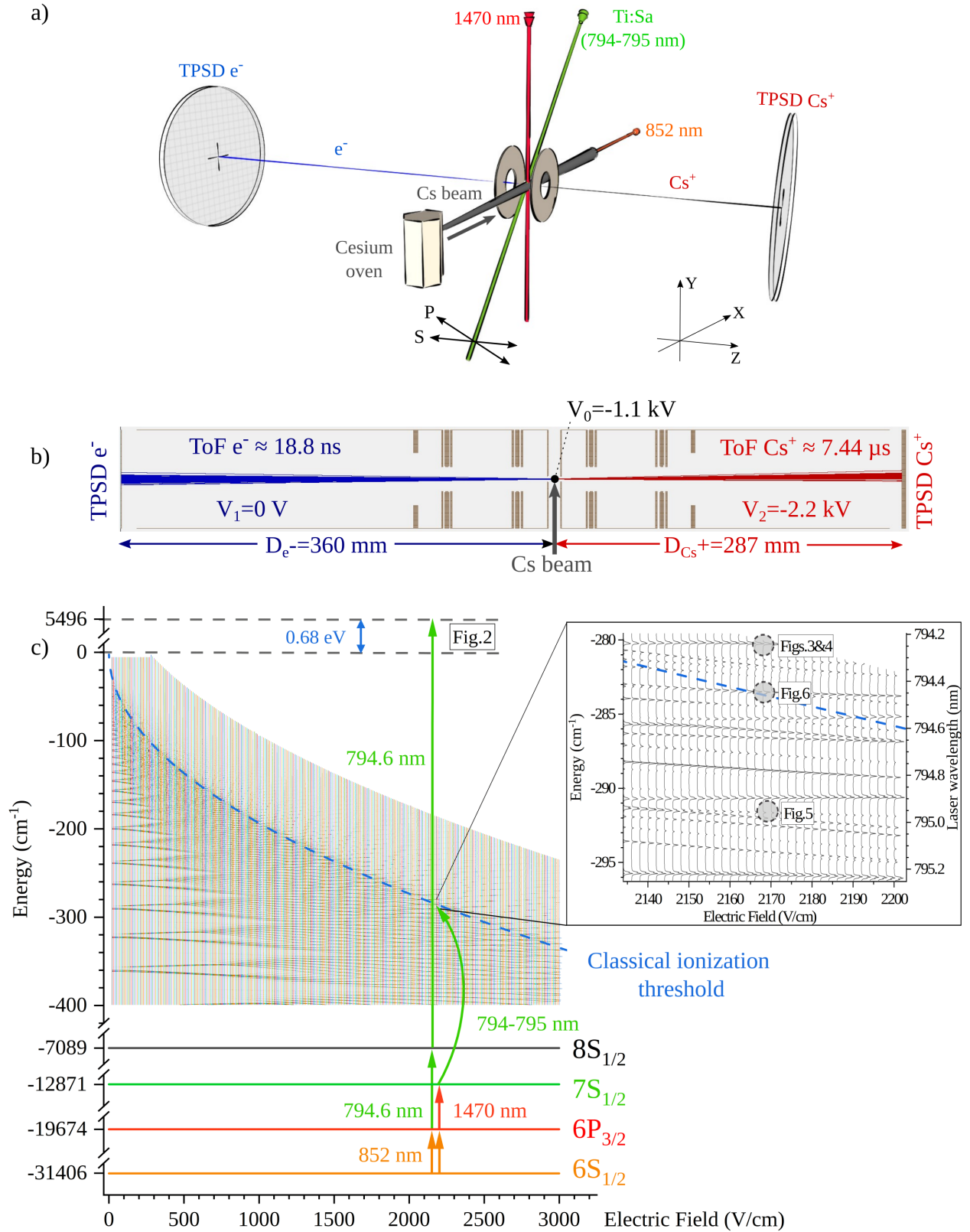


FIG. 1. a) 3-D view of the apparatus showing the cesium oven, the neutral cesium beam, the three lasers, time-and-position-sensitive detectors (TPSD) and electron and cesium ions beams. P and S arrows define the polarisation for the Ti:Sa laser, S polarization being along the Z axis. b) Planar view of the simulation c) Stark map of Rydberg states in cesium, from -400 cm^{-1} up to 100 cm^{-1} above the classical ionisation threshold (shown in blue dashed line), from 0 V/cm to 3000 V/cm , with the ionisation paths at 2170 V/cm used in this work. It is constructed from individual calculations using local-frame transformation (LFT) theory at a given electric field. The four low energy electronic states ($6S_{1/2}$, $6P_{3/2}$, $7S_{1/2}$ and $8S_{1/2}$) have negligible Stark shift. Arrows represent one photon absorption with different ionisation paths. The inset is a zoom on the Stark map, showing in details the region of further investigated ionising Rydberg states, with an explicit reference to the figures featuring the circled states.

II. SETUP

The experimental setup has been described in detail previously [19, 20] and only a brief description will be given here. It is based on a double time-of-flight (ToF) spectrometer with two TPSD at opposite ends monitored in coincidence mode. We create ion-electron pairs by excitation and ionization of a neutral Cs beam created by an effusive oven. The Cs beam enters a DC electric field produced by two parallel plates with 4 mm-diameter apertures, separated by ~ 10 mm. The holed plates also act as zoom-electrodes, allowing the imagery of the 1 mm diameter excitation region. The apertures create curved electric field lines, introducing field in-homogeneity of ~ 0.4 V/cm across the ionisation zone.

Narrowband laser excitation is performed by a three-step ($6s(F=4) \rightarrow 6p_{3/2}(F=5) \rightarrow 7s(F=4) \rightarrow \text{Rydberg}$) excitation. We can thus only excite states with total magnetic quantum number $m = 1/2$ (taking into account the electron spin). The first two lasers perform Doppler selection reducing the effect of the effusive atomic beam velocity dispersion. Low laser power ($\sim 10 \mu\text{W}$ for 852 nm, $\sim 100 \mu\text{W}$ for 1470 nm) ensures that the power-broadening of the spectroscopic lines is negligible. The only scanned laser is the Rydberg excitation ($7s \rightarrow \text{Rydberg}$) laser, a 45° angle Ti:Sa (wavelength ~ 794 nm and power ~ 100 mW), monitored using a high precision wavemeter (HighFinesse WSU-2), allowing ~ 5 MHz absolute frequency precision with sub-MHz relative precision.

Pairs of created electrons and ions are oriented by the static electric field towards the detectors, where their position and ToF are recorded. The electron detector is composed of a set of microchannel plates (MCP) and a delay line detector (DLD). The ion detector is composed of a double stack of MCPs, a phosphor screen and a CMOS camera. It uses the correlation between the brightness of the spot on the phosphor screen and the amplitude of the time signal on the MCP to correlate signals from the same event [21]. Both detectors have a position resolution of about $50 \mu\text{m}$. If the measured ToF fits within a given range around the expected value ($\simeq 200$ ns, corresponding to the spread caused by the potential difference across the ionization region), the pair is considered as coming from a unique ionization event and is labeled as coincident in time. A low counting rate (kHz range) allows image acquisition with the CMOS camera. This rate also ensures that the false coincidences are negligible.

III. CALIBRATION USING ABOVE THRESHOLD DATA

The first experimental studies on field-ionization processes in Rydberg atoms ionization were done using only spectral (from laser wavelength) and time information from ToF [1, 22]. The ToF t also gives access to the

energy of the particles, with a resolution ΔV (in eV) typically given by $\Delta V/V = 2\sqrt{2}\Delta t/t$, where V is the energy of the produced beam (~ 1 keV) and Δt (~ 100 ps) is the time resolution of the detector [23]. The ToF values (~ 19 ns for electron and $\sim 7.5 \mu\text{s}$ for the Cs^+) allow only an energy resolution at the eV scale and thus this is not very informative about the ionisation process. However, our apparatus adds an imaging capability, that gives access to the energy acquired by the particles during ionisation. Indeed the initial position of an electron is given by the detected correlated ion, and any deviation from this position is a signature of ionisation kick-energy. Any additional energy from the ionisation process will, due to energy conservation and mass difference between electrons and cesium ions, result in high electron velocities, and broadening of the image of the electrons, as well as poor correlations. For a kick-energy of 1 meV, an electron has a velocity on the order of 20 km/s and so, without any other zoom effect, the spot size of the electrons on the detector will be of the order of 4 mm, that is easily visible. The ions will almost not be affected by this energy and will fly as if they were initially at rest. For each coincident event, the X (resp. Y) coordinate of the electron is plotted with respect to the X (resp. Y) coordinate of the coincident ion, giving rise to a correlation curve for each coordinate. In our experimental conditions, the width of these correlation curves is dominated by the ionisation kick-energy [19].

This effect is first clearly visible on figure 2 where the ionisation is done far above-threshold, thus releasing the electrons with well-defined ionisation kick-energy, corresponding to the difference between the photon energy and the ionisation energy [24]. This is performed via a fortunate direct two-photon resonant ionization process (see Fig. 1(c)): one photon at 794.606 nm excites atoms in the $6p_{3/2}$ state to the $8s$ level. Excited atoms can then be ionised by a second 794.606 nm photon, with an extra energy above threshold of $\Delta V \sim 0.72$ eV (~ 0.68 eV are due to field free above threshold, the rest due to Stark shifted threshold lowering).

Ion images in both polarisation are very comparable, showing that their position are not noticeably modified by the direction of the ionisation kick. Electron images are broad and feature a clear influence of the ionising laser polarisation. The X and Y electron/ion correlation curves are thus very broad, a clear signature that additional energy is given to the electron during the ionisation. Electrons are mostly emitted along the polarization axis, introducing a clear difference between P-polarized light, that has an electric field polarized parallel to the (lasers) plane of incidence, and S-polarized that is perpendicular to this plane (see Fig. 1(a)). As expected, the S-polarized image is smooth, while the P-polarized one shows two bands (separated by ~ 13 mm) due to the electron initially ejected in the two directions along the polarization axis. Indeed as we start from the $8s$ state, and following dipolar transition rules, the free electron is emitted in a p partial wave with a photoionization dif-

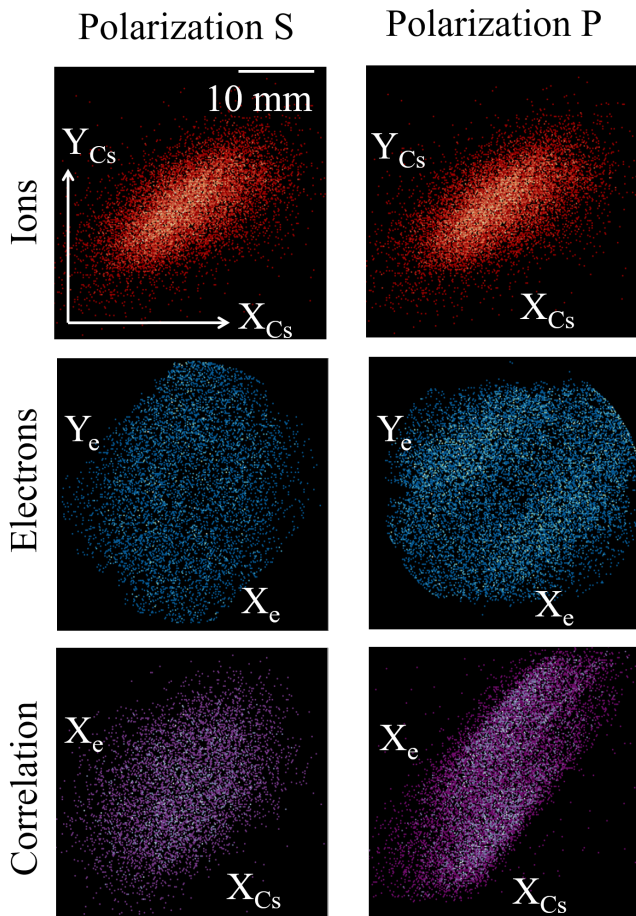


FIG. 2. Experimental images obtained with the Ti:Sa photoionization laser set with a photon energy ~ 0.72 eV above field-shifted threshold. Two different laser polarizations (S and P) are shown. The 45° angle of the laser propagation axis is clearly visible in all images. Top line: ion images. Middle line: electron images. Bottom line: corresponding (X) correlation images between electrons and ions (the Y correlations are not shown but similar).

ferential cross section of $d\sigma/d\Omega \propto \cos^2 \theta$ where θ is the polar angle (from the polarization axis).

Using an excitation from the $7s$ state to above-threshold with a blue-detuned TiSa laser up to 700 nm, we have checked the link between the width of the experimental correlation curve (see lower panel of Fig. 2) and the ionisation kick energy. We find a quadratic dependence between the energy above threshold ΔV and the FWHM of the correlation curve D : $\frac{\Delta V}{0.72 \text{ eV}} \approx \left(\frac{D}{13 \text{ mm}}\right)^2$. The quadratic dependence is expected from the simple kinetic energy formula $e\Delta V = \frac{1}{2}mv_\perp^2$ combined with the ToF that converts the radial velocity v_\perp in position. This quadratic dependence is approximated and validated down to few tens of meV of kinetic energy [24]. Below this value the classical trajectories starts to be modified by the coulomb interaction with the ionic core [25]. For even lower electron kinetic energy, electron wave

function could play a role [26]. However, because we are not in a Velocity Map Imaging configuration we are less sensitive to the wave function behaviour and, as shown below, our classical trajectory simulations are able to reproduce our results.

A first conclusion is that this ion-electron correlation scheme allows for radial energy (or velocity) measurement that an electron acquires during photo-ionisation. It clearly shows that positive energy photo-ionisation is not suitable for the production of high-quality electron beams, and that ion/electron position correlation is poor. For ionisation with low to zero extra energy (auto-ionising Rydberg states) the correlation curve is a thin line and we attain the resolution limit near 1 meV. This is confirmed by simulations showing similar line broadening than experimental ones for 1 meV electrons. Thus, without more stable voltage power supplies (the one we use have noise around 1 mV) it is difficult to know what experimentally ultimately limits the energy-resolution [19].

IV. IONISATION OF STRONGLY SHIFTED RYDBERG STATES

In this section we will use the above-described technique to study the ionisation of diverse Stark-shifted Rydberg states.

A. Short lifetime state: coupling spatial and spectral resolution

A parameter that plays an important role in the precision of the measurement is the interplay between the field inhomogeneity and the narrow spectral selection. For sufficiently narrow atomic resonances and states with strong Stark slope (dependence of energy versus field), the excitation occurs only at precise field values, so that a given laser frequency will excite atoms at different spatial location. As the electric field is created by conducting plates with circular apertures, the regions of constant field norms are hyperboloids. By carefully tuning the laser frequency (while keeping the same potentials on electrodes), we can thus select a particular region of ionisation. Two kinds of ionisation regions can be addressed: two-sheets hyperboloid symmetric around the centre of the electrodes, or one-sheet hyperboloid avoiding the central axis. These two cases are presented respectively in figures 4 and 3. Figure 3 shows the results with an excitation at 794.241 65 nm under an electric field of 2168.8 V/cm while figure 4 correspond to another state at 794.234 985 nm under the electric field of 2166.6 V/cm.

In both cases the excited states have very similar properties as shown in the LFT-Stark map, with a lifetime ~ 10 ns, short enough to allow direct auto-ionization before any visible atomic motion, but long enough in order to have a narrow resonance condition. The thinness of the correlation line indicates that the electrons are

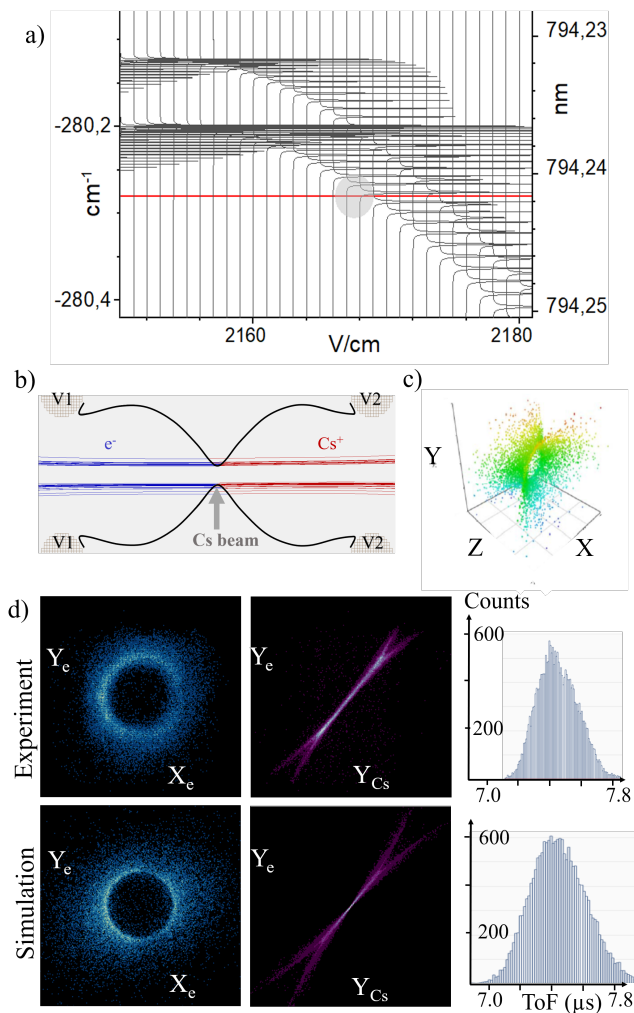


FIG. 3. Experimental and simulated results for the excitation of a fast-ionizing Stark-shifted Rydberg state. The ionising laser is set at $\lambda = 794.24165$ nm and the resonant electric field is 2169.35 V/cm. Electrode potentials are chosen to place this field value off-axis. a) LFT-Stark map around the area of interest with linewidth of the state, b) Central zoom on the Simion simulation. The field line is taken at 2169.35 V/cm, c) 3D representation of the initial ionizing point for the excited Rydberg states (the axis are 2 mm spread) d) experimental (top line) and simulated (bottom line) images, from left to right the electron image, the electron-ion (Y) correlation image and the Time of Flight (ToF) between correlated ions and electrons.

ejected with small velocity, just at the threshold.

This is clearly illustrated by simulation: in the one sheet hyperboloid case (Fig. 3) atoms are excited when their motion cross the proper (resonant electric field) one sheet hyperboloid. This occurs at many different axial positions producing only a broad ToF but in two different region radial points along their trajectories, producing, due to the cylindrical symmetry, a hollow image. On the contrary, in the two sheets hyperboloid case (Fig. 4) atoms are excited all along their trajectories, producing

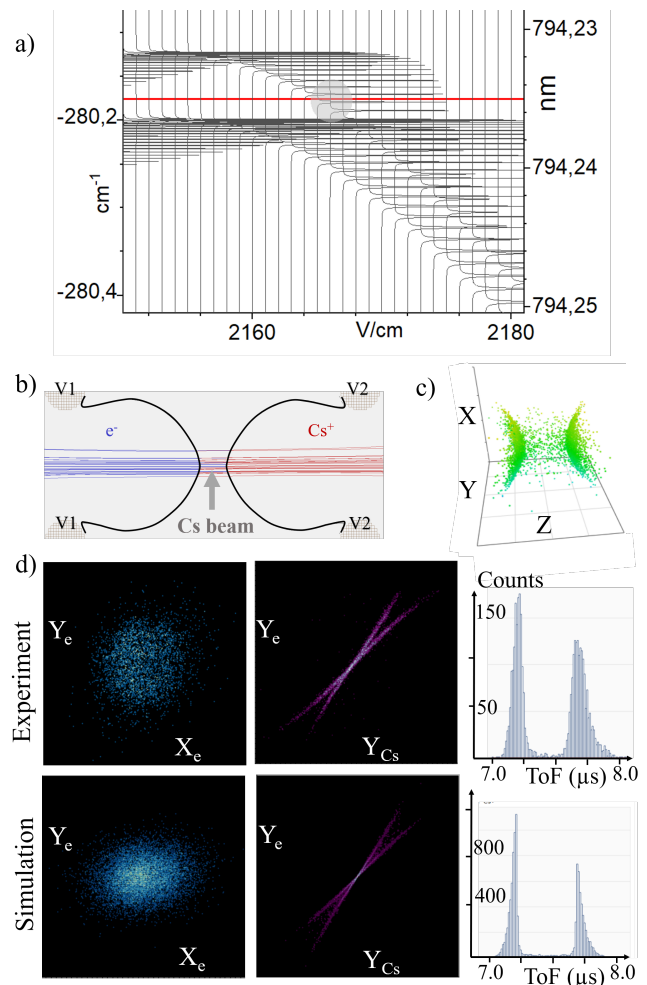


FIG. 4. Same as Fig. 3 but now after the excitation of a fast-ionizing Rydberg state resonant on electric field lines at the center of the electrodes. The field line of b) is taken at 2165.6 V/cm. The axis for the 3D representation, in c), have been modified to obtain a better view.

a single image, but at two different electric field axial positions, producing two different ion groups and so two different ToF forming two lines in the correlation curve.

1. Stark and ionization map simulation

In order to have a better understanding on the Rydberg behaviour (the Stark shift and the lifetime/ionisation rate), we have compared our results to a well established theory of photoabsorption, based on quantum defects and field-dependent frame transformation between spherical and parabolic coordinates [18]. It is able to give a Stark map (see panel a) in the lower line of figures 3 and 4, where the apparent linewidths give the ionisation rate of individual states. This theory[18] is based on a Local Frame Transformation (LFT) that is performed between the wavefunctions near the core (that

are well described by phase shifted spherical Coulomb functions) and the wavefunctions at large distances (that are well described by the solutions of the Coulomb plus Stark potential in parabolic coordinates). Thus, the transformation matrix only depends on the strength of the electric field. The resonance lifetimes are obtained in this theory through the scattering between the different parabolic channels which occurs because the low angular momentum partial waves have a phase shift. The specific properties of the atoms are incorporated through the zero field quantum defects and transition dipole matrix elements of the atom. The transition dipole matrix elements can be obtained from effective one-electron potentials, however we didn't implement them in the presented calculations.

2. Simion simulation

The simulation of the results (see middle lines of Fig. 3 and Fig. 4) is performed using the Simion[®] Ion and Electron Optics Simulator. For this purpose we use the Lua programming language allowing to transform an initial moving atom, at constant velocity \mathbf{v} , first into a Rydberg atom, then into an ion and electron pair thanks to a Monte Carlo algorithm. The atomic beam is taken as a Gaussian beam of ~ 1 mm size moving at $v_z = 200$ m/s velocity along z but, to take into account our beam geometry and the Doppler selection, with a Gaussian rms uncertainty of 5 m/s on all 3 axis. The evolution is done at every time step $dt \sim 5$ ns. The excitation to the Rydberg state (with rate Γ_{exc}) and its subsequent ionization (at rate Γ_{ion}) are calculated using the Metropolis-Hastings algorithm (the reaction is effective if Γdt is smaller than a random number taken uniformly between 0 and 1). The ion and electron trajectories are then directly handled by the Simion software. The excitation rate is taken from a perturbative two level model, giving $\Gamma_{\text{exc}} \propto \frac{I}{\delta^2 + \Gamma^2/4}$ where I is the laser intensity, δ is the detuning from resonance and Γ is the sum of the Rydberg and 7s states spontaneous emission rate (Γ_{7s}), the ionization rate (Γ_{ion}) and of the Ti:Sa laser linewidth ($\Gamma_{7s} \approx \frac{1}{50 \text{ ns}}$ and Γ_{ion} dominate). The evolution of the detuning δ and of Γ_{ion} with the electric field seen by the atoms are extracted from the corresponding LFT-Stark map (see panel (a) in the lower line of Fig. 3 and Fig. 4) and implemented using a quadratic fit in the code.

The only fitted parameter is the transition dipole matrix element, that is not provided by the LFT code. This parameter enters (squared) in the proportionality factor of the excitation rate together with the spatial dependence of the (~ 0.9 mm waist) Ti:Sa Gaussian laser intensity I .

Simulations, typically performed with 500 000 particles, agree very well with the experimental data. These simulations also help us study the excitation efficiency. For instance a neutral atom is excited to a Rydberg state with $\sim 2\%$ efficiency in the figure 4 case but $\sim 20\%$ in

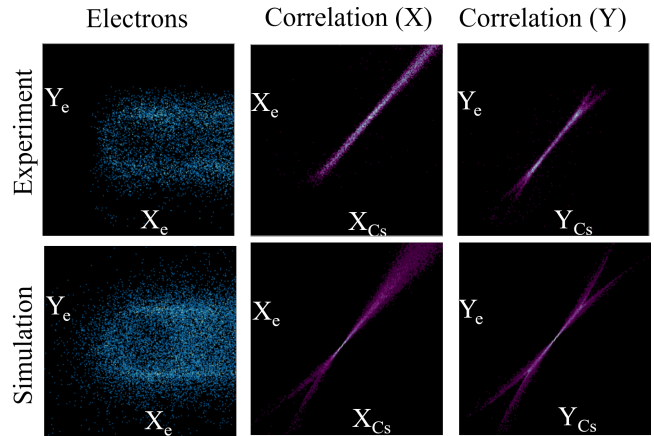


FIG. 5. Experimental and simulations results after the excitation of a long lived Rydberg state excited on the one-sheet hyperboloid. Upper (experimental results) and bottom (simulation) lines: from left to right the electron image, the X and Y electron-ion correlation images.

the figure 3 one. The higher rate is mainly due to the fact that almost all atoms cross a field value where they can be excited in the second case but the central atoms just go through the apparatus and do not find any resonant field. The efficiency is also directly visible on the experimental data, for instance with a $\sim 20\%$ reduction of the signal in the right part of the "hollow circle" data in figure 3. Indeed neutral atoms arriving in this part are the one that have not been excited in the first hyperboloid sheet.

B. Long lifetime state: motion

Due to the atomic beam velocity, a few micrometer spatial region is covered in only few tens of nanosecond. Thus, for a slower ionizing resonance (lifetime bigger than 100 ns) the narrow spatial excitation region, created thanks to the stringent spectral resolution, can still lead to a large ionisation region. This is visible in figure 5 where we excite atom with a Ti:Sa wavelength of 794.555 780 nm at a mean electric field of 2169.7 V/cm. The LFT ionization rate is only $\Gamma_{\text{ion}} \approx 1/(12 \mu\text{s})$. The rate is small enough to allow a narrow linewidth excitation and thus a resonance condition (creating the hollow structure). However, the spatial zone of ionization is very large due to the long lifetime of the state. This also broadens the correlation curves,

C. Motion induced field ionization

The lifetime of the state presented in figure 5 is long enough to allow the atoms to move to another region before their ionisation. In the case of a long-lived state

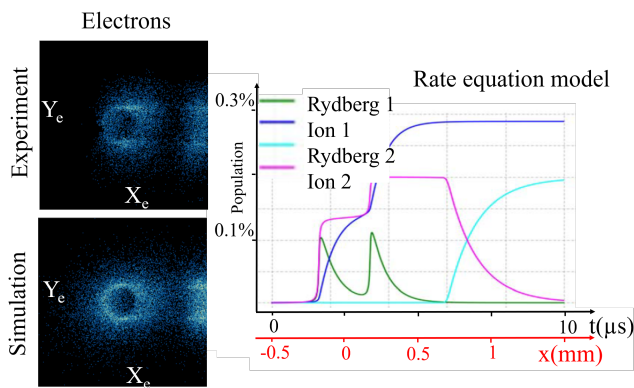


FIG. 6. Results after the excitation of a “double” state on the one-sheet field hyperboloid. Left: experiment (top) and simulation (bottom) and right: rate equation simulation for a traveling excited atom.

that has a rapidly-changing ionisation rate with the electric field [15], we could observe a sharp ionisation zone shifted from the excitation zone. We found rare occurrences of this behaviour, for example when tuning the ionising laser at 794.434 55 nm and under a 2168.8 V/cm electric field. Experimental results of this state can be found on figure 6, showing a clear distinction between excitation and ionisation.

The central spot on Figure 6 is quite similar to the one on figure 5 but stops abruptly. This clearly indicates that we excite a state that is field ionized when atoms move to higher fields. Unfortunately, if for all states presented up to now we found very good agreement between the experiment and the LFT theory, the state shown on figure 6 is not well reproduced by the LFT theory, showing an energy discrepancy of several GHz. Scanning the wavelength and field around 794.435 nm and 2170 V/cm showed the same image structure, with the excitation of a Rydberg state that ionizes “on the spot” and a second spot which is always located near the 2173 V/cm field lines. This observation possibly indicates that we excite two degenerate Rydberg states, one short lived that ionizes immediately and a second, long-lived, that ionises when reaching the 2173 V/cm field line during its flight through the excitation region.

We have thus simulated this situation using a 60% excitation for the unstable state with a lifetime of 550 ns and a 40% excitation for the stable state that ionizes at a 2173 V/cm field. To take this into account, we use a Gauss error function dependence of Γ_{ion} , as a function of the field, from 0 to 1400 ns with a rms $\sigma \sim 0.1$ V/cm. These values scale with our choice of a typical Stark shift of 0.007 cm^{-1} per 1 V/cm. The agreement between the experiment and the simulation is very good, as seen on figure 6. However, our interpretation is still questionable because it is not supported by the LFT Stark maps.

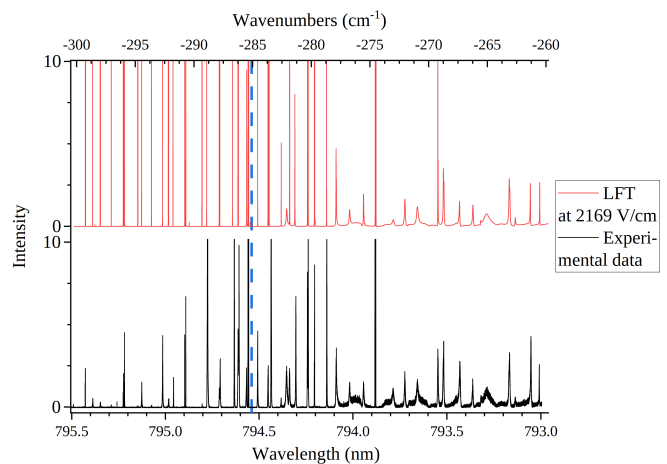


FIG. 7. Comparison of experimental and theoretical (LFT) photoionisation scans. The classical ionisation field threshold is indicated by a blue dashed line. Intensity scales are arbitrary, and both spectra are cut from the top in order to better see the low intensity lines.

D. Critical comparison of experimental data with LFT theory

As mentioned before, and as shown on figure 8, the LFT code [18] at our disposal accurately predicts the energies and lifetimes of Stark states both below the shifted-threshold and way over it. Figure 7 shows a comparison between LFT scans and experimental scans over a large energy range (1.2 THz) around the field-shifted threshold, that is at -285.082 cm^{-1} at the field of 2169 V/cm. The direct comparison shows very good agreement both on the energy positions and linewidths of probed states, both below and above threshold. The intensity of experimental peaks artificially decreases below -290 cm^{-1} because of long-lived states, leading to low electron collection. Even more, comparing intensities is tricky for two other reasons: we did not implement field-free transition dipoles in the code; and we compare experimental ionisation intensity with theoretical absorption, which are linked by ionisation rates. This means that the relative intensities differences between experiment and theory (in particular in the low-energy, low ionisation rates region) can not directly be attributed to defects in the theory. However, in regions with ionisation efficiency close to 1 (above the classical threshold), the raw LFT-intensity still compares very well with experiments.

To improve the comparison, in particular on the linewidths, from qualitative to quantitative, we performed the same scan on another set-up (described in [15]), with smaller field inhomogeneities and tighter-focused lasers. A comparison of these data with the corresponding LFT spectrum is shown in figure 8.

We improved the comparison by convoluting the theoretical spectra with an estimation of the field inhomogeneity in the ionisation region. The result is a very good

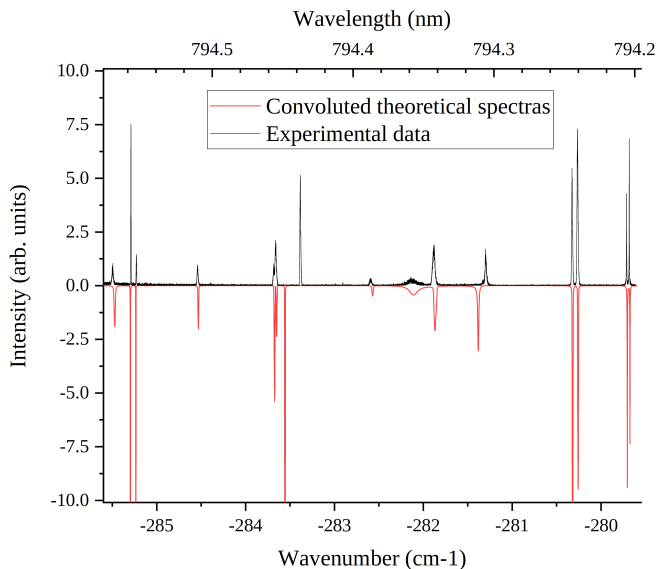


FIG. 8. Comparison of computed and experimentally acquired photo-absorption spectra at $F = 2172.3$ V/cm. The theoretical spectrum is a weighted sum of spectra at different electric field values to compensate for the finite extension of the ionisation zone (and thus the electric field inhomogeneity). The code is accurate on the position, Stark slopes and natural linewidth of all peaks but the peculiar one corresponding to the state studied on figure 6 visible at ~ -283.3 cm^{-1} .

agreement on the predicted energies of most states, with mean errors of 200 MHz. Two instances of higher discrepancy (at -283.5 cm^{-1} and -281.2 cm^{-1}) in the GHz range were nevertheless present, indicating critical points in the LFT (the first one corresponds to the state presented on figure 6). The observed linewidths are in very good agreement, even for states whose energy is poorly predicted. This confirms that LFT can be used to predict energies and ionisation rate in this energy range.

The accuracy of the LFT theory was already ascertained in many systems [27–29], but to our knowledge this is the first time that this theory is compared with experimental results on cesium with good energy resolution [30]. These calculations were considered as reliable enough to be used for an electric field calibration, with an estimated precision better than 1 V/cm. As the code uses sets of quantum defects as input, we wanted to rule out the possible role of inaccurate quantum defects in the aforementioned large discrepancies, so we performed additional calculations with different sets of quantum defects.

The main set of quantum defects was constructed from the most recent experimental values and completed with older measurements [31–34]. It was compared with the quantum defects set used in the software and python library Alkali Rydberg Calculator [32, 33] for ease of comparison with other published data. We also tested the influence of each value not present in the most precise reference [31]. This analysis revealed that the amplitude

of quantum defects errors, that would be responsible for the observed inaccuracies, are too big to be credible. It means that the match between the calculated and observed states positions is not primarily dependent on the precision of the quantum defects values, and we conclude that the errors come solely from the theory. This study also proves that, when the quantum defects for $d_{3/2}$ states is changed, of all the states presented in figure 8, the most affected by this change are the one with the initial higher discrepancy. This is a strong indication that the LFT theory, while accurate on most states in this energy field range, particularly lacks accuracy with states with strong d-component. This resonates with recent findings that the LFT does not, in some cases, conserve the total angular momentum [35].

A more exact theory named Generalized Local-Frame-Transformation (GLFT), based on R-matrix local frame transformation, has been shown to improve the accuracy of computed photoionization Stark spectra by two or three orders of magnitude, down to a few tens of MHz [35]. We believe that the lack of accuracy in the present calculations could be detrimental to our future experimental effort and thus that it will become interesting to implement GLFT or any other supposedly more precise theoretical framework [27].

V. CONCLUSION

In conclusion we have studied many cases of Rydberg field-ionisation, from way above threshold (very unstable states) to way below threshold (meta-stable states) including crossing, tunneling or interference narrowing effects. By combining the 2D spatial image and the ToF we have a full 3D information on the initial ion-electron position: the image gives access to the transverse position where the ToF refers to the axial position.

Excitation of states with lifetime bigger than 100 ns (slow ionisation) converts the spectral resonant excitation to a spatial selection thanks to the inhomogeneous electric field. This can be used to produce narrow excitation, or ionization zone much smaller than the laser spot. This is an interesting situation where the spatial position, and thus the ion electrical potential energy, can be modified simply by changing the laser frequency. The use of ion-electron correlation allows good energy resolution for the ionisation kick-energy, and already indicates the potentiality for the use of such states to produce very monochromatic electron or ion beams [15, 19, 36]. In particular this technique should allow us to identify states that experience a rapidly changing ionisation rate when evolving in an inhomogeneous electric field.

Standard photoabsorption theory based on quantum defects and field-dependent frame transformation was found to agree well with our experimental results, both for the energy positions and for the linewidths/ionisation rates of the Rydberg-Stark states, for all the data except two peaks that shows several GHz discrepancy. Updating

this code to the more recent and more precise GLFT[35] could resolve these discrepancies.

(grant number ANR-10-LABX-0039-PALM) and the ANR-HREELM. We thank F. Robicheaux for providing us with the simulation code and for fruitful discussions.

VI. ACKNOWLEDGEMENTS

This work was supported by the Fond Unique Interministériel (IAPP-FUI-22) COLDFIB, the labex PALM

-
- [1] T. F. Gallagher, *Rydberg Atoms* (Cambridge University Press, Cambridge, 1994).
 - [2] T. W. Ducas, M. G. Littman, R. R. Freeman, and D. Kleppner, *Phys. Rev. Lett.* **35**, 366 (1975).
 - [3] M. G. Littman, M. M. Kash, and D. Kleppner, *Physical Review Letters* **41**, 103 (1978).
 - [4] E. Luc-Koenig *et al.*, *Le Journal de Physique Colloques* **43**, C2 (1982).
 - [5] V. S. Lisitsa, *Soviet Physics Uspekhi* **30**, 927 (1987).
 - [6] S. Feneuille, S. Liberman, E. Luc-Koenig, J. Pinard, and A. Taleb, *J. Phys. B* **15**, 1205 (1982).
 - [7] D.-H. Yang, D. Lieberman, P. van der Straten, T. Bergeman, and H. Metcalf, *Phys. Rev. A* **40**, 5026 (1989).
 - [8] J.-Y. Liu *et al.*, *Phys. Rev. Lett.* **55**, 189 (1985).
 - [9] P. McNicholl, T. Bergeman, and H. J. Metcalf, *Phys. Rev. A* **37**, 3302 (1988).
 - [10] W. van de Water, D. R. Mariani, and P. M. Koch, *Phys. Rev. A* **30**, 2399 (1984).
 - [11] A. Nussenzweig, E. E. Eyler, T. Bergeman, and E. Pollock, *Phys. Rev. A* **41**, 4944 (1990).
 - [12] G. Kuik, W. Vassen, C. Lahaije, and W. Hogervorst, *Zeitschrift für Physik D Atoms, Molecules and Clusters* **39**, 127 (1997).
 - [13] C. Chardonnet, D. Delande, and J. C. Gay, *Opt. Commun.* **51**, 249 (1984).
 - [14] C. Chardonnet, D. Delande, and J. C. Gay, *Phys. Rev. A* **39**, 1066 (1989).
 - [15] E. Mofarej *et al.*, *Phys. Rev. A* **95**, 043409 (2017).
 - [16] M. L. Zimmerman, M. G. Littman, M. M. Kash, and D. Kleppner, *Phys. Rev. A* **20**, 2251 (1979).
 - [17] J. Grimm *et al.*, *Phys. Rev. A* **96**, 013427 (2017).
 - [18] D. A. Harmin, *Phys. Rev. A* **30**, 2413 (1984).
 - [19] C. Lopez, A. Trimeche, D. Comparat, and Y. Picard, *Physical Review Applied* **11**, 064049 (2019).
 - [20] A. Trimeche, C. Lopez, D. Comparat, and Y. Picard, *arXiv preprint arXiv:2003.02186* (2020).
 - [21] X. Urbain *et al.*, *Review of Scientific Instruments* **86**, 023305 (2015).
 - [22] M. G. Littman, M. M. Kash, and D. Kleppner, *Phys. Rev. Lett.* **41**, 103 (1978).
 - [23] K. Medjanik *et al.*, *Journal of Synchrotron Radiation* **26**, 1996 (2019).
 - [24] W. Engelen, E. Vredenburg, and O. Luiten, *Ultramicroscopy* **147**, 61 (2014).
 - [25] T. Barillot *et al.*, *The Journal of Chemical Physics* **147**, 013929 (2017).
 - [26] C. Nicole, H. Offerhaus, M. Vrakking, F. Lépine, and C. Bordas, *Phys. Rev. Lett.* **88**, 133001 (2002).
 - [27] G. D. Stevens *et al.*, *Phys. Rev. A* **53**, 1349 (1996).
 - [28] M. Grütter, O. Zehnder, T. P. Softley, and F. Merkt, *J. Phys. B* **41**, 115001 (2008).
 - [29] L. B. Zhao, I. I. Fabrikant, M. L. Du, and C. Bordas, *Phys. Rev. A* **86**, 1045 (2012).
 - [30] F. Robicheaux, *Phys. Rev. A* **56**, 4032 (1997).
 - [31] J. Deiglmayr *et al.*, *Physical Review A* **93**, 013424 (2016).
 - [32] C. J. Lorenzen and K. Niemax, *Zeitschrift für Physik A Atoms and Nuclei* **315**, 127 (1984).
 - [33] K.-H. Weber and C. J. Sansonetti, *Phys. Rev. A* **35**, 4650 (1987).
 - [34] P. Goy, J. M. Raimond, G. Vitrant, and S. Haroche, *Phys. Rev. A* **26**, 2733 (1982).
 - [35] P. Giannakeas, C. H. Greene, and F. Robicheaux, *Phys. Rev. A* **94**, 013419 (2016).
 - [36] M. Mankos *et al.*, *Ultramicroscopy* **207**, 112848 (2019).